ACS OMEGA

Open Access

http://pubs.acs.org/journal/acsodf

Article

Structural Investigation of Schiff Base Ligand and Dinuclear Copper Complex: Synthesis, Crystal Structure, Computational, and Latent Fingerprint Analysis

Udaya Kumar A. H, Mahesha, Pampa K. J, Nanishankar V. Harohally, Chethan Krishnamurthy, Keshavayya Jathi, Akil Ahmad, Mohammed B. Alshammari, and Neratur Krishnappagowda Lokanath*

Cite This: *ACS Omega* 2024, 9, 30109−30119

Read Online

ACCESS | Metrics & More | Article Recommendations | Supporting Information

ABSTRACT: The structural studies of the fluorinated Schiff base ligand and its copper complex were synthesized and characterized by Fourier transform infrared, UV-visible, and photoluminescence spectroscopy. Single-crystal X-ray diffraction analysis unveils a dinuclear copper complex arising from double bridging acetate anions to copper ions that are chelated by the tridentate Schiff base ligand Cu(LS). The trigonality index τ_5 of 0.080 indicates a distorted square pyramidal coordination geometry for the metal. The SL ligand and complex exhibit intra- and intermolecular interactions, leading to unique supramolecular architectures. The structural changes between the free halogenated Schiff base ligand and upon coordination with the metal were extensively studied by experimental and theoretical approaches. The intra- and intermolecular interactions have been analyzed by Hirshfeld surface and quantum theory of atoms in molecules analysis, and the enrichment ratio highlights the most favored interactions in the formation of molecular packing. The chemical and physical properties, such as the HOMO − LUMO energy gap, chemical reactivity, and electron density topology, are studied using density functional theory studies. In addition, the Schiff base ligand compound is used to study the latent fingerprint analysis.

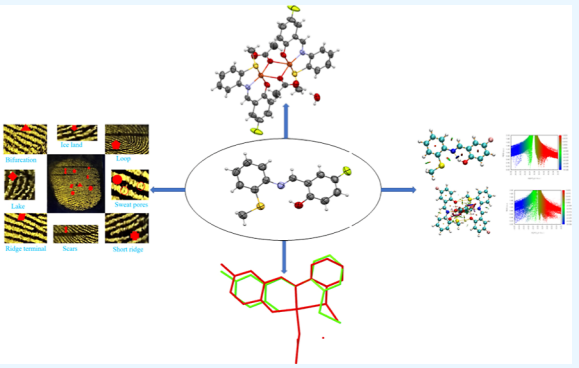

1. INTRODUCTION

Schiff bases are typical organic substances that can be synthesized by single-step condensation of a primary amine and a carbonyl compound, typically an aldehyde/ketone, which reacts with the amino group to form an azomethine chain.[1] The Schiff base having O, N, and S donor groups is gaining interest in the coordination chemistry field because of their ability to form stable coordination complexes.[2] In particular, thioanisole and halogen-based benzaldehyde provide N, O, and S donor atoms that are known to exhibit good fluorescent and antimicrobial properties.[3] The thioanisole, comprising a benzene ring and a thiomethyl ($-SCH_3$) group, stands as a pivotal benzene derivative with a flexible substituent. The molecular structure of thioanisole has been determined by various spectroscopic characterization. The proposed conformational states for thioanisole include both planar and nonplanar conformers, particularly concerning the internal rotation of the thiomethyl group around the $C(sp^2)-S$ bond.[4] These Schiff base ligands and their metal complexes have fascinating properties in various fields, such as catalysts in the organic synthesis in the production of pharmaceuticals, dyes, fluorescence agents and polymers.[5−7] They also exhibit activity against a wide range of microorganisms such as bacteria, fungi, and viruses by disrupting the microbial cell membrane.[8,9]

Furthermore, they demonstrate anticancer efficacy against breast, lung, and colon cancer cells by targeting cell lines.[10] The Schiff base metal complexes have a flexible structure that allows them to adjust their conformations to the coordination geometry of the metal ion. These structural modifications can change the electronic and magnetic properties of the metal complex, making it useful for various applications.[11,12] The remarkable metal ion properties are highly influenced by intra- and intermolecular interaction, including a hydrogen bond, $\pi\cdots\pi$ stacking, coordinate bond, and electron transfer interaction.

Additionally, the formation of metal complexes enhances their ability to form supramolecular structures through hydrogen bonding and other intermolecular interactions.[13]

Received: September 29, 2023
Revised: June 14, 2024
Accepted: June 14, 2024
Published: July 1, 2024

These phenomena led to their use in the design of functional materials such as liquid crystals, gels, and polymers.[14,15] Schiff bases and their metal complexes are also known for their fluorescent properties, which make them useful in various applications such as sensors, imaging reagents, and molecular probes.[16,17]

Herein, we report the synthesis of a novel Schiff base ligand and its copper complex ($[Cu_2(SL_2)(CH_3COOH)_2]$) characterized by Fourier transform infrared (FTIR) spectroscopy, and X-ray diffraction studies confirmed their crystal structure. In addition, the effect of metal complex formation on structural and supramolecular architecture was also studied. The Hirshfeld surface (HS) and Quantum theory of atoms in molecules (QTAIM) analysis were used to study the intra- and intermolecular interaction. The density functional theory DFT studies were carried out to explore the electronic properties of the SL ligand and metal complex. Furthermore, latent fingerprint (LFP) analysis for the Schiff base ligand was performed.

2. RESULTS AND DISCUSSION

2.1. X-ray Crystallographic Studies. The molecular structure of the Schiff base ligand (SL) and its copper complex was determined by single crystal X-ray diffraction, and the ORTEP drawings, along with the atom numbering scheme, are illustrated in Figure 1. Both the ligand and complex crystallize in the monoclinic space group *C*2/*c*. The Schiff ligand comprises the methylsulfonylbenzene ring that connects the 4-fluorophenol via an azomethine chain (−C7−H7═N1-) and presents an E configuration with respect to the C7═N1 bond. The azomethine torsion angle C6−C7═N1−C8, of 176.1(2)°, is representative of a *+antiperiplanar* (*+ap*) conformation. The dihedral between the two aromatic rings of the Schiff base ligand is found to be 22.62°, which indicates a nonplanar molecule. The molecule SL exhibits an intramolecular O1−H1···N1 hydrogen bond to form an S(6) H-bonded ring synthon (Table 1 and Figure S1).

The dinuclear metal complex is centrosymmetric, being located about an inversion center. The crystallographic independent copper ion is coordinated by the tridentate Schiff base ligand through the O, N, and S donors. The deprotonated oxygen and nitrogen atoms form a six-membered chelating ring, whereas nitrogen and sulfur form a five-membered one. Two symmetry-related Cu(SL) units are bridged by carboxylate anions through oxygen O2 and O2′ forming a Cu_2O_2 rhombus core.

The crystallographically independent copper ion adopts a five coordination geometry, characterized by a trigonality index τ^5 of 0.080, which indicates a slightly distorted square pyramidal geometry [$\tau_5 = (\beta - \alpha)/(60°)$, where β and α are the largest angles N1−Cu1−O2 and O1−Cu1−S1, being 0 for a regular square-based pyramidal geometry].[18]

The μ_2-bridging oxygen of acetate is coordinated to one copper ion at the square pyramidal basal plane and at the apical position to the symmetry-related metal with Cu−O2 and Cu^i−$O2^i$ bond distances of 1.972(3) and 2.403(3) Å, respectively. The two coordination polyhedra share an edge to form a rhombus core. The interionic distance between the copper atom is 3.392 Å is longer than similar compounds which are present in the multinuclear metalloenzymes showing oxidase activity.[19,20] An overlay of the crystal structures of the free ligand and upon coordination shows the structural changes due to the formation of the complex (Figure S2). All of the

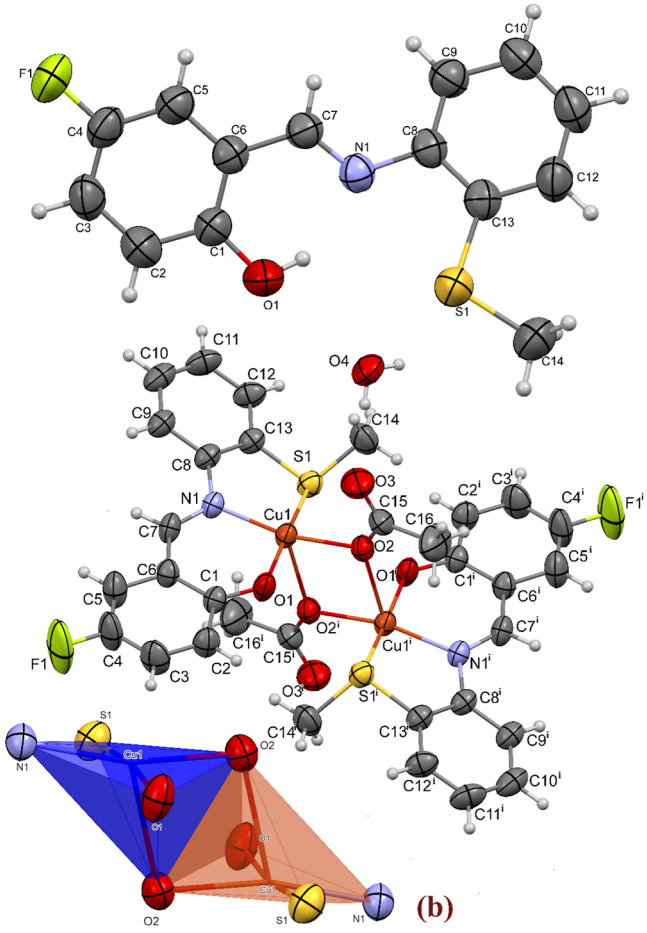

Figure 1. (a) ORTEP view (thermal ellipsoids drawn at 50% probability) of the ligand SL and (b) its copper complex along with polyhedra representation of coordination geometry (i symmetry code = $-x + 1, -y, -z + 1$).

geometrical parameters of both ligand and complex are tabulated in Tables S1−S3.

2.1.1. Supramolecular Architecture Description and 3D HS Analysis. Intermolecular interactions play a crucial role in stabilizing the crystal structure of the ligand and its copper complex, giving rise to supramolecular assemblies in the crystalline phase. The SL molecules form cyclic inversion dimer through C14−H14A···S1 interactions, with a distance of 3.694(9) Å and an angle of 100° (1/2 − *x*, *y*,1 − *z*). This interaction is visually emphasized by a red spot on the 3D HS of the ligand, as illustrated in Figure S3a. Furthermore, this interaction forms an $R_2^2(6)$ supramolecular ring synthon and is interconnected by C14−H14B···C11 [3.593(4) Å, 144°, 1 − *x*, −*y*, 1 − *z*] interactions to form a 1-D infinite chain, as shown in Figure 2a. The 1D chains are interconnected through C8···C7 interaction to form a 2-D supramolecular architecture (Figure 2b). Moreover, the ligand exhibits a C4−F1···Cg(1) interaction, where Cg represents the centroid of the ring C1−C6, with a distance of 3.9067(2) Å. The presence of this interaction is highlighted by distinctive bow and tie shapes on the shape index of the ligand (Table 2 and Figures S4,S5).

In the copper complex, the lattice water molecule, located on a twofold axis, interconnects to the complex unit via an O4−H4···O3 [3.819(5) Å, 159° 1 − *x*,−*y*,1 − *z*] interaction to form a 1D chain (Figure 3a). Additionally, the interaction is highlighted by deep red spots on the HS of the copper

https://doi.org/10.1021/acsomega.3c07536
ACS Omega 2024, 9, 30109−30119

Table 1. Hydrogen Bond Geometry for the SL Ligand and Complex[a]

compound	interaction	type	D−H (Å)	H···A (Å)	D···A (Å)	D−H···A (deg)
SL ligand	O1−H1···N1	intra	0.82	1.92	2.638(2)	145.00
complex	O4−H4···O3[1]	inter	0.85	1.97	2.819(5)	179.00
	C5−H5···O4[2]	inter	0.93	2.58	3.460(6)	159.00
	C14−H14B···F1[3]	inter	0.96	2.53	3.387(6)	149.14

[a]Symmetry code: $1 - x,-y,1 - z^1$; $1 - x,1 - y,1 - z^2$; $1/2 + x,1/2 - y,1/2 + z^3$.

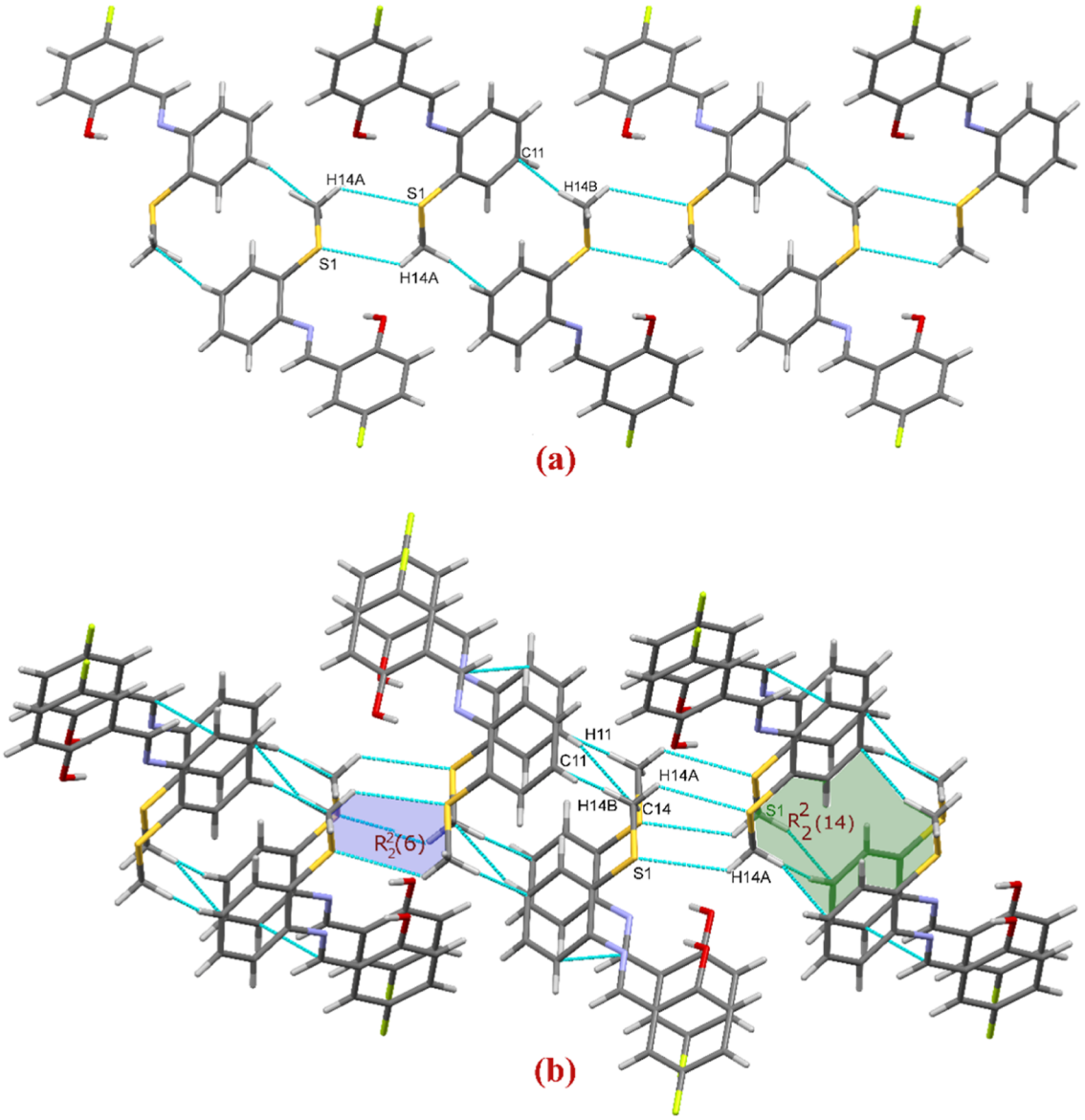

Figure 2. 1D molecular packing of (a) ligand and (b) copper complex showing intermolecular interactions.

Table 2. C−F···Cg Interaction Geometry for SL Ligand and Complex[a]

compound	interaction	X···Cg (Å)	Y−X···Cg (Å)	Y···Cg (Å)	Y−X, Pi (deg)
SL ligand	C4−F1···Cg(1)[1]	3.9067(2)	95.01(1)	4.251(3)	0.98
complex	C4−F1···Cg(5)[2]	3.596(5)	128.70	4.572(7)	35.07

[a]Symmetry code: $x - 1 + y, z^1$; $1 - x, y,1/2 - z^2$.

complex around O3, as illustrated in Figure S3 (b). The C9−H9···O3(3.304(6) Å, 130.43°, $1 - x,1 - y,1 - z$), O4−H4···O3, and C5−H5···O4 [3.460(6)Å, 159°, $1 - x,1 - y,1 - z$] interaction and $R_3^2(13)$ ring synthon interconnect a 1-D chain to form the 2D sheet (Figure 3b), and dark red spots on the HS of the complex indicate a strong hydrogen bond interaction (Figure S3b). The C14−H14B···F1[3.387(6) Å, 149.14°, $1/2 + x,1/2 - y,1/2 + z$] along with other interactions, forms a 3D supramolecular topology Table 2. The complex exhibits C4−F1···Cg(5) (Cg is the centroid of the ring C8−C13) with an

https://doi.org/10.1021/acsomega.3c07536
ACS Omega 2024, 9, 30109−30119

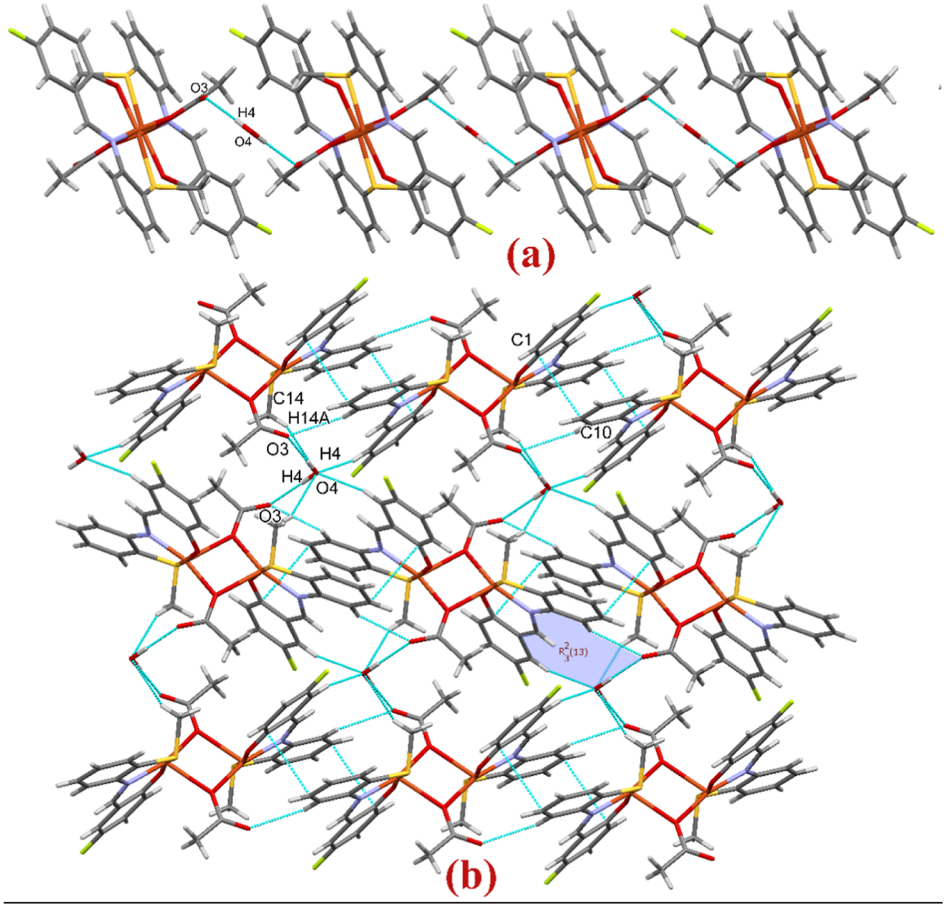

Figure 3. 2D molecular packing of (a) the ligand and (b) the copper complex showing intermolecular interactions.

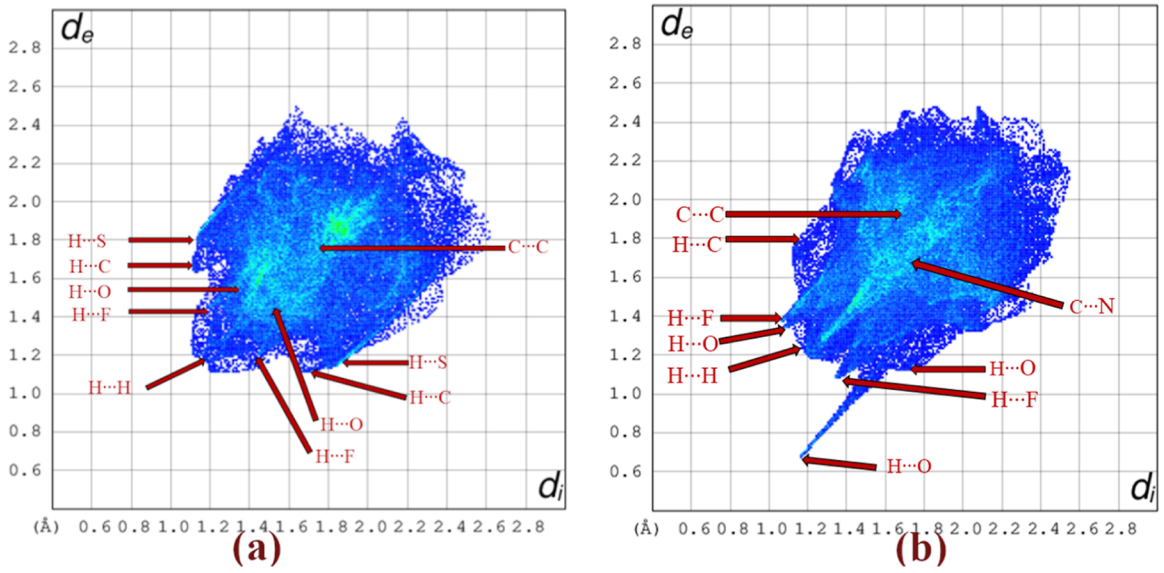

Figure 4. 2D fingerprint plot of the (a) ligand and (b) copper complex.

interaction distance of 3.596(5) Å and also supported by the shape index of the complex showing bow and tie shapes in blue and red color (Table 2 and Figures S5 and S6). The slipped $\pi\cdots\pi$ interaction was observed between the chelating ring Cg(3) and Cg(5) rings [where Cg(3) and Cg(5) are the centroids of the ring Cu−O1−C1−C6−C7−N1 and C8−C13] interaction with a distance of 3.823(4) Å. Moreover, the $\pi\cdots\pi$ stacking interaction is corroborated by the curvedness. The increased number of blue lines on the curvedness plot of the copper complex signifies the nonplanarity of the molecule upon complexation, as shown in Figure S6d.

2.2. 2D Fingerprint and Enrichment Ratio Analyses. The 2D fingerprint plot of the SL ligand and the copper complex provides quantitative information about intramolec-

https://doi.org/10.1021/acsomega.3c07536
ACS Omega 2024, 9, 30109−30119

Table 3. Ligand and Copper Complex Bonding Interactions with the Corresponding Topological Parameters

compound	bonding interaction	ρ (r)	$\nabla 2\rho(r)$	$G(r)$	$V(r)$	$H(r)$	E_{int} (kcal/mol)
SL	O1−H1···N1	0.0414	0.1052	0.0384	−0.0353	−0.005	−11.0788
complex	O4−H4···O3	0.0173	0.3136	0.0323	−0.0314	−0.001	−9.8170
	C14−H14A···O4	0.0064	0.0227	0.0047	−0.0036	0.0010	−1.1401
	O1···S1	0.0063	0. 0241	0.0051	−0.0042	0.0009	−1.3283

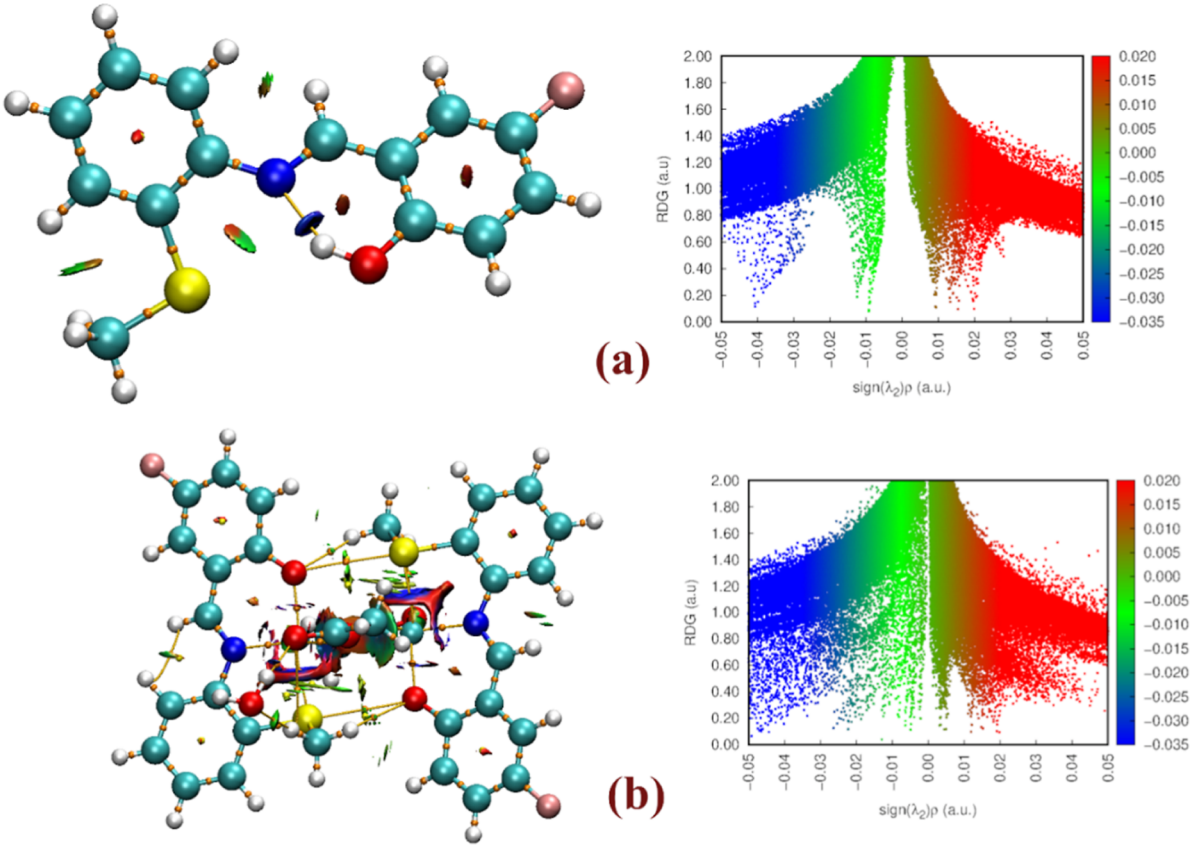

Figure 5. Combined QTAIM and NCI (3D and 2D) plots for (a) the SL ligand and (b) the complex.

ular interaction (Figure 4). In ligand and complex, the hydrogen atom generates 39.4 and 44.1% of the molecular surface, respectively. The complex shows a high percentage of contribution H···H, and this is due to the presence of water as a lattice solvent forms only hydrogen-based interaction. The H···H characteristic peaks observed in the 2D graph at d_e + d_i1.2 Å and two peaks present in the vicinity of d_e + d_i1.4 Å correspond to the H···F interaction (Figure S6). The two symmetrical spikes for H···O interaction were observed for the ligand (d_e + d_i1.4 Å). In the copper complex, the asymmetric peaks are observed at d_e + d_i1.4 and 1.2 Å observed (Figure S7). The copper complex consisting of water molecules in the lattice enhances H···O interaction by 5.6%. The actual contact hydrogen-based interaction in both compounds is more than 60% of the molecular surface. Carbon is the second most contributing element in the ligand, while fluorine is the second most contributing element in the copper complex. The C···H (d_e + d_i1.7 and 1.8 Å for ligand and complex) actual contacts represent the C−H···π interaction and the C−C (d_e + d_i1.8 and 1.9 Å for ligand and complex) represents π···π interaction. The enrichment ratio (ER) calculation highlights the H···H contacts (ER_{HH} = 1), which turn out to be more favored in the molecular packing of ligand and complex. The π···π stacking is enriched in the copper complex (ER_{CC} = 2.1) than in the ligand (ER_{CC} = 1.6). The S···H interaction is higher in the ligand (ER_{SH} = 1.5) than the copper complex indicates (ER_{SH} = 1.3) and helps to stabilize 1D packing via the ring synthon. The other interactions listed in Table S4 having greater ER values are also favored and stabilize the structures.

2.3. QTAIM Analysis. QTAIM is a theoretical framework for analyzing the electronic structure of molecules. It involves the analysis of the electron density distribution within a molecule and identification of critical points in the electron density as bond critical points and ring critical points. The value of the electron density, $\rho(r)$ and its first derivative, the sign of $\nabla^2\rho$, at the bond critical point can provide information about the nature of bonding type and strength in a molecule. In ligand, the O1−H1···N1 interaction is highlighted by the blue circular disc, indicating strong intramolecular interaction, and the interatomic interaction energy is −46.421 kJ mol^{-1} (Table 3 Figure 5a). The green iso-surface indicated the other dihydrogen interaction. In copper complex, water molecules present in the lattice form the O4−H4···O3 and C14−H14A···O4 interaction have interatomic interaction energies of −9.817 and −1.1401 kJ mol^{-1} (Table 3 and Figure 5b). The O1···S1 interactions interconnect the inversion-symmetry-generated molecule with interaction energies of −1.3283 kJ mol^{-1}. Around the coordination geometry, the Cu1−O2 coordination

https://doi.org/10.1021/acsomega.3c07536
ACS Omega 2024, 9, 30109−30119

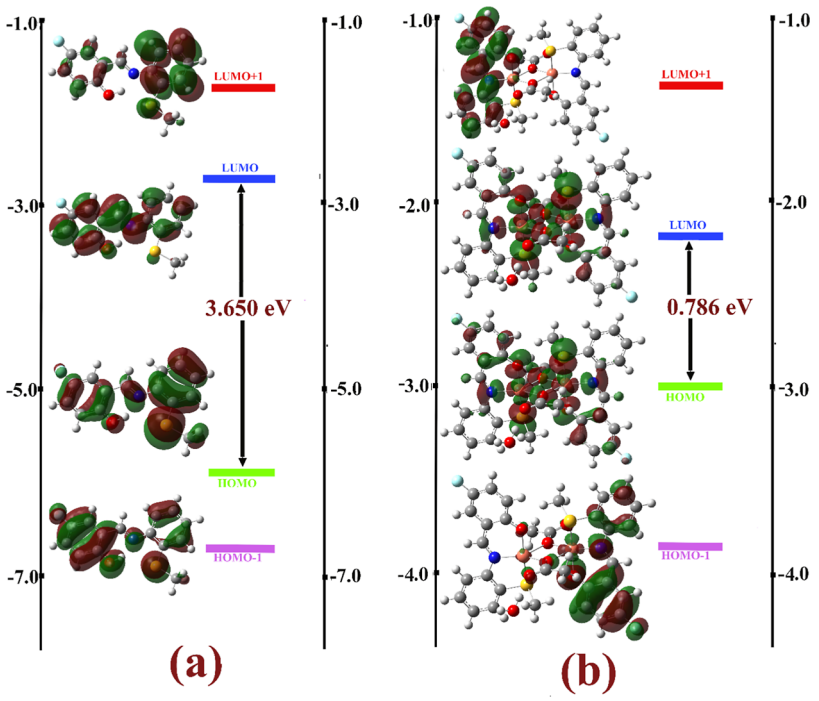

Figure 6. Frontier HOMO − LUMO molecular orbitals of (a) ligand and (b) complex with an energy gap.

bonds show mixed blue-green color, indicating a weak coordination bond and the formation four-membered ring forms ring strain indicated by the red color. The 2D plot indicates the strength of hydrogen and various noncovalent interactions. The formation of the copper complex leads to the more scattered blue and green color in the 2D graph, indicating more hydrogen and vdW intramolecular interactions. In between the two copper atoms, the green-red colored iso-surface is present, which indicates the metal−metal interaction. The red color is also present in 3D and 2D graphs, indicating that steric repulsive interaction is dominant due to the formation of chelation and intramolecular interaction rings.

2.4. Quantum Computational Analysis. Quantum computational analysis is very useful in studying the electronic structure and properties of the molecule. The SL ligand and copper complex are optimized with ground state energies of −1168.96 and 3262.02 hartree, respectively. The optimized structure and crystal structure of both compounds are overlaid and yield good rmsd values of 0.266 and 0.600, respectively, for ligand and copper complex (Figure S8). In addition, bond length, bond angle, and torsion angles were also compared and tabulated in Tables S1−S3. The frontier molecular orbital analysis provides a HOMO − LUMO energy gap. The ligand has an energy gap of 3.650 eV and the formation of copper complex leads to a significantly reduced energy gap with a value of 0.786 eV (Figure 6). The result indicates that the metal complex is more reactive compared to the ligand. The HOMO − LUMO is delocalized all over the molecule in the ligand, whereas, in the complex, they are mainly localized over the coordination sphere. The global and local reactive parameters calculated on the basis of the energy gap for the ligand and metal complex are tabulated in Table 4. The most negative regions (red) of the molecular electrostatic potential (MEP) maps for the ligand are mainly localized over the O1 atoms, indicating that they are the most suitable active site for the coordination bond (Figure S9a). In the metal complex, the lattice water molecule shows a red region and indicates the most suitable active site for the electrostatic active site. Both ligand and complex fluorine atoms are yellow around the atom and blue at the top of the atom, indicating anisotropic charge distribution (Figure S9b). The C−H bonds in each molecule are blue, indicating the most probable nucleophilic sites.

Table 4. Global and Local Reactive Parameters of the SL Ligand and Complex

parameter	SL ligand	complex
E_{HOMO}	−5.9256	−5.2719
E_{LUMO}	−2.2751	−4.4855
energy gap (eV)	3.6504	0.7864
ionization energy (eV)	5.9256	5.2719
electron affinity (eV)	2.2751	4.4855
electronegativity (eV)	4.1003	4.8787
chemical potential (eV)	−4.1003	−4.8787
global hardness (eV)	1.8252	0.3932
global softness (eV^{-1})	0.5479	2.5432
electrophilicity index (eV)	4.6057	30.2667

NBO calculation provides natural electronic configuration (NEC), and natural and Mulliken charges (Figure S10), which are tabulated in Tables S5 and S6. By comparing the free metal ion NEC of Cu^{2+} is [core] $4S^{1}3d^{8}$ and upon complex formation, the NEC changes to [core]4s(0.28)3d(9.52)4p (0.41). The comparison of natural and Mulliken charges between the ligand and metal complex and the NEC indicates the delocalization effect and charge transfer interaction in the molecular system. The stabilization energies E(2) for the donor (filled) and acceptor (unfilled) Lewis-type NBOs are listed in Table S7. The ligand exhibits the highest stabilization energy of 465 kcal/mol for the LP(3)(O1)→ LP*x(3)(H1) interaction. In contrast, the copper complex shows the highest interaction energy, 444.67 kcal/mol, for LP(3)(O4)→ LP*(1)(H4) interaction.

https://doi.org/10.1021/acsomega.3c07536
ACS Omega 2024, 9, 30109−30119

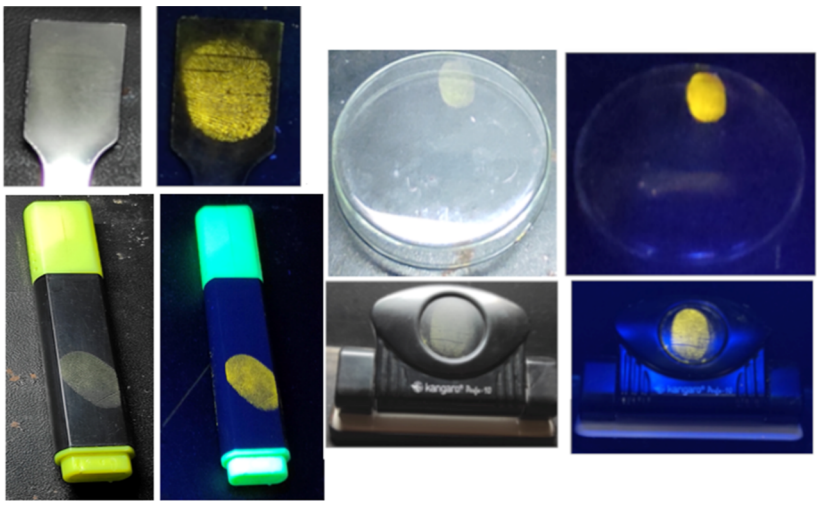

Figure 7. LFPs were captured using SL on different surface materials of a spatula, coin, glass, marker pen, and punching machine.

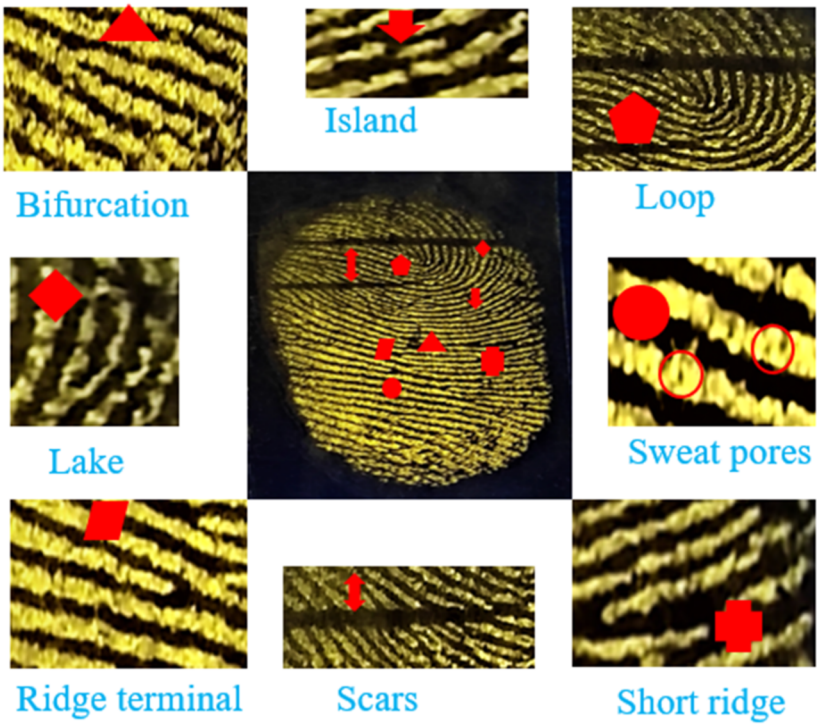

Figure 8. Various LFPs ridge notations on spatula under UV-light (365 nm).

2.5. LFP Analysis. Fingerprint analysis is a powerful tool used in forensic science for the identification of individuals. Schiff base ligands selectively bind to the amino acids and fatty acids present in the fingerprint residue, leading to the formation of a fluorescent complex. This complex can then be visualized under UV light, providing a clear and distinct image of the fingerprint. LFPs were obtained by pressing the fingers against several surfaces such as coins, glass, plastic (marker pen), punching machine, and spatula surfaces of substrates. The powder dusting method was utilized to obtain the LFPs by using an SL molecule (Figure 7). There is no background interference when observing the ridges at levels 1 to 3, such as bifurcation, lake, island, sweat pores, ridge terminal, short ridge, loop, and scares (Figure 8). The zoomed images of fingerprints at higher resolution can provide valuable information. Hence, our Schiff base compounds in fingerprint analysis are promising and could potentially improve the accuracy and reliability of forensic investigations.

3. CONCLUSIONS

This research work describes a comprehensive understanding of the synthesized Schiff base ligand and its copper complex through various spectroscopic, structural, and computational studies. HS analysis, 2D fingerprint plots, and ER analysis support the supramolecular architecture formed by various interactions in the crystal structure. The QTAIM analysis provides intermolecular interaction energies of the O1−H1···N1 interaction in the ligand and lattice solvent exhibits the O4−H4···O3 interaction energies present in the complex. The DFT studies show the formation of copper complex significantly reduced to the HOMO − LUMO energy gap. The ligand exhibits fluorescent properties and is effectively

https://doi.org/10.1021/acsomega.3c07536
ACS Omega 2024, 9, 30109−30119

Scheme 1. Synthesis Scheme for SL Ligands and Copper Complex

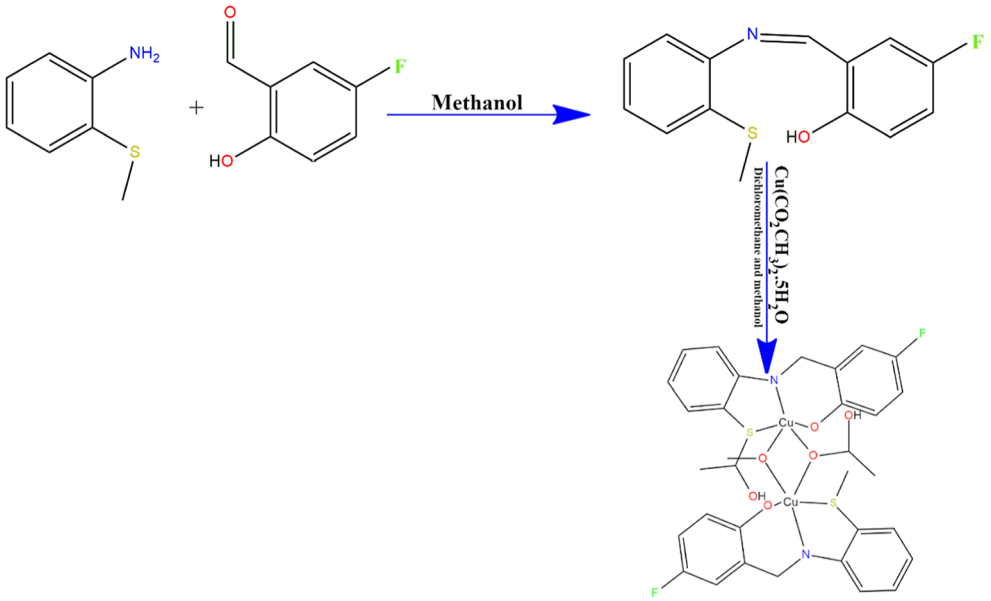

used to study LFP analysis. The bright and high-resolution fingerprints are promising and could potentially improve the accuracy and reliability of forensic investigations.

4. EXPERIMENTAL SECTION

4.1. Materials and Instrumentation. All of the starting materials and solvents used for synthesis are analytical grade and procured from Sigma-Aldrich and TCI India and used without any further purification. The FT-IR analyses were measured with a FTIR (PerkinElmer Spectrum Version 10.03.09) and the spectrum is presented in Figure S11. The fluorescence spectra (Figure S12a) and UV−visible spectra (Figure S12b) of the Schiff base ligand are obtained using a JASCO FP-8300 Fluorescence spectrometer and Beckman coulter DU730 spectrometer. The morphology and elemental composition of SL ligand and copper complex were determined by the scanning electron microscopy and EDAX analysis.

4.2. Synthesis and Crystal Growth. *4.2.1. Synthesis of SL ((E)-2-(((2-(tert-Butylthio)phenyl)imino)methyl)-4-fluorophenol).* 2-(Methylthio) aniline (1 mmol) was dissolved in methanol (10 mL) and was added to 10 mL of methanolic solution of 5-fluorosalicylaldehyde (1 mmol). The yellow mixture was refluxed at 60 °C for 3 h and then allowed to cool at room temperature. The obtained yellow precipitate is filtered out, dissolved in the methanol solution, and allowed to evaporate slowly. After 30 days, yellow, colored needle-shaped crystals are grown in mother liquor solution. The synthesis scheme for SL ligands is represented in Scheme 1.

4.2.2. Synthesis of Copper Complex (([Cu_2(SL)$_2$(CH_3COOH)$_2$])). The SL ligand (1 mmol) was dissolved in the 10 mL dichloromethane solvent, and copper acetate mono hydrate (1 mmol) was dissolved separately in 20 mL of methanol. Then, both solutions were mixed dropwise at 60 °C with constant stirring, and the green-colored precipitate was obtained after 6 h. Furthermore, the green-colored solution was filtered and kept for slow evaporation. After 40 days, rectangular green crystals were obtained. The synthesis scheme for copper complex is represented in Scheme 1.

4.3. X-ray Crystallographic Studies. Suitable single crystals of the Schiff base ligand and its copper complex were isolated from the crystallizing solvent. X-ray diffraction intensity data were collected using a Rigaku XtaLAB mini diffractometer equipped with a charge-coupled device detector and Mo−Kα radiation (λ = 0.71073 Å). The quality of the mounted crystals was initially investigated using 12 diffraction frames, and then, a complete data collection was carried out by using the *CrystalClear-SM Expert 2* package.[21] Data were integrated and processed with the *d*TREK* program, and an empirical absorption correction was applied (*RAXshape* program). The structures were solved using the SHELXT program using the intrinsic phasing method[22] and refined with the SHELXL[23] (implemented in *Olex-2 software*[24]). With anisotropic non-hydrogen atoms and H atoms geometrically located at the ideal positions. Details of the crystal data and refinement parameters are given in Table 5. Bond lengths and angles were calculated using *PLATON* software,[25] and ORTEP pictures and packing diagrams were drawn by *MERCURY* software.[26]

4.4. HS Analysis. The 3D HSs and 2D fingerprint plots were used to quantify the nature of the intermolecular interaction. HS of the ligand and metal complex was generated by uploading the.cif file into *CrystalExplorer 17.5* software.[27] The d_{norm} is the normalized contact used to visualize the nature of the intermolecular interaction. The color code is used in order to show the strength of noncovalent interaction. Intermolecular interactions are indicated by red, white, and blue spots, respectively, when their lengths are less than, equal to, and higher than van der Waal radii. The shape index has red and blue triangles, which indicates the $\pi\cdots\pi$ and C−H$\cdots\pi$ interaction. The 2D fingerprint plot provides quantitative analysis of intermolecular contacts exhibited by the molecular structure and is used to quantify the individual contribution between the pair of atoms. The 2D fingerprint plot is obtained by reducing HSs and binning d_i and d_e into discrete intervals, producing a 2D plot with an interval of 0.02 Å.[28] The ER is a useful tool which indicates the most favored interaction in the crystal structure. For any given pair of elements, an ER greater than unity indicates a high chance of forming interactions in

https://doi.org/10.1021/acsomega.3c07536
ACS Omega 2024, 9, 30109−30119

Table 5. SL Ligand and Copper Complex Crystallographic Data and Refinement Parameters

compound	SL	copper complex
CCDC deposit no	2239313	2239314
empirical formula	$C_{14}H_{12}FNOS$	$C_{32}H_{29}F_2Cu_2\ N_2O_7S_2$
formula weight	261.31	782.81
crystal system, space group	monoclinic, *I2/a*	monoclinic, *C2/c*
unit cell dimensions	18.1129(12)	18.687(19)
a (Å)	4.9416(3)	10.235(10)
b (Å)	29.068(2)	17.382(17)
c (Å)	90.00	90.00
α (deg)	105.322(8)	91.392(14)
β (deg)	90.00	90.00
γ(deg)	90.00	90.00
volume (Å^3)	2509.3(3)	3324(6)
Z	8	4
density (calculated) in Mg m^{-3}	1.383	1.564
absorption coefficient (mm^{-1})	0.256	1.466
F_{000}	1088	1596
crystal size (mm^3)	0.20 × 0.26 × 0.24	0.36 × 0.34 × 0.16
θ range for data collection (deg)	2.906 to 56.314	3.16 to 27.51
index ranges	$-23 \le h \le 23$ $-6 \le k \le 3$ $-37 \le l \le 37$	$-13 \le h \le 24$ $-13 \le k \le 13$ $-21 \le l \le 22$
reflections collected	10,206	9392
independent reflections	2903 [R_{int} = 0.0988]	3788 [R_{int} = 0.0703]
data/restraints/parameters	2903/0/165	3788/0/218
goodness-of-fit on F^2	1.057	1.073
final [$I > 2\sigma(I)$]	*R*1 = 0.0592, w*R*2 = 0.1479	*R*1 = 0.0489, w*R*2 = 0.1267
R indices (all data)	*R*1 = 0.0910, w*R*2 = 0.1798	*R*1 = 0.0699, w*R*2 = 0.1434
largest diff. peak and hole (eÅ^{-3}) Å^{-3}	0.28 and −0.29	0.741 and −0.730

the crystal structure, while a value of less than unity indicates a less favored interaction.[29,30] The energy framework analysis was carried out to determine the molecular interaction energies with a graphical representation.

4.5. QTAIM Analysis. QTAIM analysis is a very useful tool to investigate the topological and geometrical features of electron density. In addition, the intra- and intermolecular interaction and the strength of hydrogen bonds were also studied. Initially, the.wfn file is generated using an optimized structure and fed into the *Multiwfn software*.[31] Using the topology analysis module, all the critical points are explored, and corresponding topological parameters are calculated. In addition to topology analysis, reduced density gradient analysis is used to study the noncovalent interaction, and it enables us to visualize the various interactions such as hydrogen bond, van der Waal (Vdw) interaction, and steric effects. The output file obtained from the topological analysis is visualized (3D and 2D maps) using *VMD* and *Gnuplot software*.[32,33]

4.6. Quantum Computational Analysis. The molecular geometry optimization of SL ligand and its complex was carried out using *Gaussian 16W* computational software.[34] Both the ligand and metal complex are optimized using the B3LYP functional along with the 6-311+g(d,p) basis set, and for the metal complex mixed basis set, (6-311+G-(d,p)+LANL2DZ) was used.[35] The vibrational frequency calculation was carried out for the optimized structure to ensure that the structure is in local minima on the potential energy surface by observing zero negative frequency. *Gauss view* software is used to display the frontier molecular orbitals, such as the highest occupied molecular orbital (HOMO), lowest unoccupied molecular orbital (LUMO), and molecular electrostatic potential (MEP).[36] Using the HOMO − LUMO energy gap, we determined the global and local parameters of the molecule. NBO calculation for the optimized structure was carried out using *NBO 3.1* software.[37]

4.7. LFP Analysis. In this study, prior to collecting the fingerprints, the individual washed his hands with soap and water, then rubbed his forehead, and pressed his fingers onto various substrates ion, glass, plastic (marker pen), punching machine, and spatula surfaces. The fingerprints were developed by using the classical powder-dusting method. First, the synthesized SL ligand powders were applied by using a feather brush and evenly distributed onto the fingerprints. The excess powder was then gently removed by using the brush. The resulting fluorescent patterns of the fingerprints were observed under a 365 nm light lamp and photographed using a digital camera.[38,39]

■ ASSOCIATED CONTENT

Data Availability Statement

CCDC 2239313 and 2239314 contain the supplementary crystallographic data of the SL ligand and copper complex. These data can be obtained free of cost via http://www.ccdc.cam.ac.uk/conts/retrieving.html, or from the Cambridge Crystallographic Data Centre, 12 Union Road, Cambridge CB2 1EZ, UK; fax: (+44) 1223−336−033; or e-mail: deposit@ccdc.cam.ac.uk.3.

Supporting Information

The Supporting Information is available free of charge at https://pubs.acs.org/doi/10.1021/acsomega.3c07536.

Spectral data; intramolecular ring synthons in the SL ligand; crystal structure overlay; d_{norm} mapped HS of the ligand and copper complex; C-F···Cg interaction for the SL ligand and complex; bond lengths comparison; comparison of angles and torsion angles; HS shape index; 2D fingerprint plot; percentage of Hirshfeld contact surfaces; overlay view of crystal structure; molecular electrostatic potential map; comparison of natural and Mulliken charges of the SL ligand and complex; natural atomic charges and natural electron configuration of the ligand and its complex; and second-order perturbation theory analysis (PDF)

■ AUTHOR INFORMATION

Corresponding Author

Neratur Krishnappagowda Lokanath − *Department of Studies in Physics, University of Mysore, Mysuru 570 006 Karnataka, India;* orcid.org/0000-0003-2773-2247; Email: lokanath@physics.uni-mysore.ac.in

Authors

Udaya Kumar A. H − *Department of Studies in Physics, University of Mysore, Mysuru 570 006 Karnataka, India*

Mahesha − *Department of Physics, SJCE, JSS Science and Technology University, Mysore 57006 Karnataka, India*

Pampa K. J − *Department of Biotechnology, University of Mysore, Mysuru 570 006 Karnataka, India*

https://doi.org/10.1021/acsomega.3c07536
ACS Omega 2024, 9, 30109−30119

Nanishankar V. Harohally − *Department of Spice and Flavour Science, CSIR-CFTRI, Mysuru 570 020 Karnataka, India;* orcid.org/0000-0003-2306-5897
Chethan Krishnamurthy − *Department of Chemistry, Jnanasahyadri, Kuvempu University, Shivamogg 577451 Karnataka, India*
Keshavayya Jathi − *Department of Chemistry, Jnanasahyadri, Kuvempu University, Shivamogg 577451 Karnataka, India*
Akil Ahmad − *Department of Chemistry, College of Sciences and Humanities, Prince Sattam Bin Abdulaziz University Al-Kharj, Al-Kharj 11892, Saudi Arabia*
Mohammed B. Alshammari − *Department of Chemistry, College of Sciences and Humanities, Prince Sattam Bin Abdulaziz University Al-Kharj, Al-Kharj 11892, Saudi Arabia*

Complete contact information is available at: https://pubs.acs.org/10.1021/acsomega.3c07536

Notes

The authors declare no competing financial interest.

■ ACKNOWLEDGMENTS

The authors are thankful to the DST-FIST(SR/FST/PSI-119/2019), National Single Crystal Diffractometer Facility, DoS in Physics, CPEPA, IOE and DST-PURSE, Vijnana Bhavan, University of Mysore, Mysuru. The author, U.K.A.H., would like to thank the DST-KSTePS Government of Karnataka for providing the fellowship.

■ REFERENCES

(1) Jia, Y.; Li, J. Molecular assembly of Schiff base interactions: construction and application. *Chem. Rev.* **2015**, *115* (3), 1597−1621.
(2) Vyas, K. M.; Joshi, R. G.; Jadeja, R.; Ratna Prabha, C.; Gupta, V. K. Synthesis, spectroscopic characterization and DNA nuclease activity of Cu (II) complexes derived from pyrazolone based NSO-donor Schiff base ligands. *Spectrochim. Acta, Part A* **2011**, *84* (1), 256−268.
(3) Udaya Kumar, A.; Pampa, K.; Harohally, N. V.; Das, D.; Ghosh, B. N.; Lokanath, N. Structural studies of Schiff base ligand and its copper complexes: Solvents effect in 1-D polymeric and monomeric copper (II) complexes, computational and sensing studies. *Mater. Chem. Phys.* **2023**, *306*, 128031.
(4) Hoshino-Nagasaka, M.; Suzuki, T.; Ichimura, T.; Kasahara, S.; Baba, M.; Kawauchi, S. Rotationally resolved high-resolution spectrum of the S 1-S 0 transition of jet-cooled thioanisole. *Phys. Chem. Chem. Phys.* **2010**, *12* (40), 13243−13247.
(5) Liu, X.; Hamon, J.-R. Recent developments in penta-hexa-and heptadentate Schiff base ligands and their metal complexes. *Coord. Chem. Rev.* **2019**, *389*, 94−118.
(6) Kajal, A.; Bala, S.; Kamboj, S.; Sharma, N.; Saini, V. Schiff bases: a versatile pharmacophore. *J. Catal.* **2013**, *2013*, 1−14.
(7) Kaczmarek, M. T.; Zabiszak, M.; Nowak, M.; Jastrzab, R. Lanthanides: Schiff base complexes, applications in cancer diagnosis, therapy, and antibacterial activity. *Coord. Chem. Rev.* **2018**, *370*, 42−54.
(8) Elangovan, N.; Thomas, R.; Sowrirajan, S. Synthesis of Schiff base (E)-4-((2-hydroxy-3, 5-diiodobenzylidene) amino)-N-thiazole-2-yl) benzenesulfonamide with antimicrobial potential, structural features, experimental biological screening and quantum mechanical studies. *J. Mol. Struct.* **2022**, *1250*, 131762.
(9) Abdel-Rahman, L. H.; Abu-Dief, A. M.; Ismael, M.; Mohamed, M. A.; Hashem, N. A. Synthesis, structure elucidation, biological screening, molecular modeling and DNA binding of some Cu (II) chelates incorporating imines derived from amino acids. *J. Mol. Struct.* **2016**, *1103*, 232−244.
(10) Kirishnamaline, G.; Magdaline, J. D.; Chithambarathanu, T.; Aruldhas, D.; Anuf, A. R. Theoretical investigation of structure, anticancer activity and molecular docking of thiourea derivatives. *J. Mol. Struct.* **2021**, *1225*, 129118.
(11) Long, J. Luminescent Schiff-base lanthanide single-molecule magnets: The association between optical and magnetic properties. *Front. Chem.* **2019**, *7*, 63.
(12) Miyasaka, H.; Matsumoto, N.; Ōkawa, H.; Re, N.; Gallo, E.; Floriani, C. Complexes derived from the reaction of manganese (III) Schiff base complexes and hexacyanoferrate (III): syntheses, multi-dimensional network structures, and magnetic properties. *J. Am. Chem. Soc.* **1996**, *118* (5), 981−994.
(13) Chaudhry, M. T.; Patrick, B. O.; Akine, S.; MacLachlan, M. J. Noncooperative guest binding by metal-free [2+ 2] Schiff-base macrocycles. *Org. Biomol. Chem.* **2022**, *20* (42), 8259−8268.
(14) Thaker, B.; Patel, P.; Vansadiya, A.; Kanojiya, J. Substitution effects on the liquid crystalline properties of thermotropic liquid crystals containing Schiff base chalcone linkages. *Mol. Cryst. Liq. Cryst.* **2009**, *515* (1), 135−147.
(15) Jiang, J.; Dong, R. Y.; MacLachlan, M. J. Lyotropic liquid crystallinity in mixed-tautomer Schiff-base macrocycles. *Chem. Commun.* **2015**, *51* (90), 16205−16208.
(16) Berhanu, A. L.; Mohiuddin, I.; Mohiuddin, I.; Malik, A. K.; Aulakh, J. S.; Kumar, V.; Kim, K. H. A review of the applications of Schiff bases as optical chemical sensors. *Trac. Trends Anal. Chem.* **2019**, *116*, 74−91.
(17) Qin, J.-c.; Fan, L.; Yang, Z.-y. A small-molecule and resumable two-photon fluorescent probe for Zn2+ based on a coumarin Schiff-base. *Sens. Actuators, B* **2016**, *228*, 156−161.
(18) Blackman, A. G.; Schenk, E. B.; Jelley, R. E.; Krenske, E. H.; Gahan, L. R. Five-coordinate transition metal complexes and the value of $\tau 5$: observations and caveats. *Dalton Trans.* **2020**, *49* (42), 14798−14806.
(19) Mahesha; Krishnegowda, H. M.; Karthik, C. S.; Kudigana, P. J.; Mallu, P.; Neratur, L. K. μ-phenoxide bridged mixed ligand Cu (II) complex: Synthesis, 3D supramolecular architecture, DFT, energy frameworks and antimicrobial studies. *Polyhedron* **2020**, *185*, 114571.
(20) Klabunde, T.; Eicken, C.; Sacchettini, J. C.; Krebs, B. Crystal structure of a plant catechol oxidase containing a dicopper center. *Nat. Struct. Biol.* **1998**, *5* (12), 1084−1090.
(21) *Expert C.S.*, v2. 1. Rigaku Americas: The Woodlands, TX, USA, 2015.
(22) Sheldrick, G. M. SHELXT-Integrated space-group and crystal-structure determination. *Acta Crystallogr., Sect. A: Found. Adv.* **2015**, *71* (1), 3−8.
(23) Sheldrick, G. M. Crystal structure refinement with SHELXL. *Acta Crystallogr., Sect. C: Struct. Chem.* **2015**, *71* (1), 3−8.
(24) Dolomanov, O. V.; Bourhis, L. J.; Gildea, R. J.; Howard, J. A.; Puschmann, H. OLEX2: a complete structure solution, refinement and analysis program. *J. Appl. Crystallogr.* **2009**, *42* (2), 339−341.
(25) Spek, A. Single-crystal structure validation with the program PLATON. *J. Appl. Crystallogr.* **2003**, *36* (1), 7−13.
(26) Macrae, C. F.; Edgington, P. R.; McCabe, P.; Pidcock, E.; Shields, G. P.; Taylor, R.; Towler, M.; van de Streek, J. Mercury: visualization and analysis of crystal structures. *J. Appl. Crystallogr.* **2006**, *39* (3), 453−457.
(27) Mackenzie, C. F.; Spackman, P. R.; Jayatilaka, D.; Spackman, M. A. CrystalExplorer model energies and energy frameworks: extension to metal coordination compounds, organic salts, solvates and open-shell systems. *IUCrJ* **2017**, *4* (5), 575−587.
(28) Udaya Kumar, A. H.; Kumara, K.; Harohally, N. V.; Pampa, K. J.; Lokanath, N. K. Square Planar trans-N2O2 Cu (II) Complex: Synthesis, Crystal Structure, Hirshfeld Surface, DFT, Antimicrobial and Docking Studies. *ChemistrySelect* **2021**, *6* (24), 6240−6255.
(29) Jelsch, C.; Ejsmont, K.; Huder, L. The enrichment ratio of atomic contacts in crystals, an indicator derived from the Hirshfeld surface analysis. *IUCrJ* **2014**, *1* (2), 119−128.
(30) Hema, M.; Hema, M. K.; Karthik, C. S.; Pampa, K. J.; Mallu, P.; Lokanath, N. K. Solvent induced mononuclear and dinuclear mixed

ligand Cu (II) complex: structural diversity, supramolecular packing polymorphism and molecular docking studies. *New J. Chem.* **2020**, *44* (41), 18048−18068.
(31) Lu, T.; Chen, F. Multiwfn: A multifunctional wavefunction analyzer. *J. Comput. Chem.* **2012**, *33* (5), 580−592.
(32) Humphrey, W.; Dalke, A.; Schulten, K. VMD: visual molecular dynamics. *J. Mol. Graph.* **1996**, *14* (1), 33−38.
(33) Racine, J. *gnuplot 4.0: A portable interactive plotting utility*; Wiley Online Library, 2006.
(34) Frisch, M. J.; Trucks, G. W.; Schlegel, H. B.; Scuseria, G. E.; robb, M. A.; Cheeseman, J. R.; Scalmani, G.; Barone, V.; Mennucci, B.; Petersson, G. A.; et al. *Gaussian09*. R. A.1; gaussian, Inc.: Wallingford CT, 2009, pp 150−166.*121*
(35) Chiodo, S.; Russo, N.; Sicilia, E. LANL2DZ basis sets recontracted in the framework of density functional theory. *J. Chem. Phys.* **2006**, *125* (10), 104107.
(36) Dennington, R.; Keith, T. A.; Millam, J. M. *GaussView 6.0. 16*; Semichem Inc.: Shawnee Mission, KS, USA, 2016.
(37) Glendening, E.; Reed, A.; Carpenter, J.; Weinhold, F. *NBO*. Version 3.1, 1998. Google Scholar There is no corresponding record for this reference.
(38) Hai, J.; Wang, H.; Sun, P.; Li, T.; Lu, S.; Zhao, Y.; Wang, B. Smart responsive luminescent aptamer-functionalized covalent organic framework hydrogel for high-resolution visualization and security protection of latent fingerprints. *ACS Appl. Mater. Interfaces* **2019**, *11* (47), 44664−44672.
(39) Dong, X.-Y.; Niu, X.-Q.; Zhang, Z.-Y.; Wei, J.-S.; Xiong, H.-M. Red fluorescent carbon dot powder for accurate latent fingerprint identification using an artificial intelligence program. *ACS Appl. Mater. Interfaces* **2020**, *12* (26), acsami.0c01972−29555.

https://doi.org/10.1021/acsomega.3c07536
ACS Omega 2024, 9, 30109−30119